Effectiveness of 2D Digital Image Correlation in Capturing the Fracture Behavior of Sheet Metal Alloys

Akshat Agha[1]

[1]FADI-AMT LLC

December 20, 2022

Effectiveness of 2D Digital Image Correlation in Capturing the Fracture Behavior of Sheet Metal Alloys

Akshat Agha
FADI-AMT LLC, Greenville, SC, USA 29607
aagha@clemson.edu | +1 3363464213 | ORCiD 0000-0001-9992-1114

SAE International Journal of Materials and Manufacturing (SAE-JMM)

Suggested Citation: *Agha, A., "Effectiveness of 2D Digital Image Correlation in Capturing the Fracture Behavior of Sheet Metal Alloys," SAE Int. J. Mater. Manf. 16(2):2023, https://doi.org/10.4271/05-16-02-0009.*

ABSTRACT

It is a consensus in academia and the industry that 2D Digital Image Correlation (2D-DIC) is inferior to a stereo DIC for high-accuracy material testing applications. It has been theoretically established by previous researchers that the 2D-DIC measurements are prone to errors due to the inability of the technique to capture the out-of-plane motion/rotation and the calibration errors due to lens distortion. Despite these flaws, 2D-DIC is still widely used in several applications involving high accuracy and precision, for example- studying the fracture behavior of sheet metal alloys. It is, therefore, necessary to understand and quantify the measurement errors induced in the 2D-DIC measurements. In this light, the presented work attempts to evaluate the effectiveness of 2D-DIC in mechanical testing required for the generation of fracture strain vs. triaxiality curve for sheet metal. This work presents a direct comparison of fracture strains obtained by 2D-DIC and stereo DIC for four loading conditions (uniaxial tension, plane strain, shear, and balanced biaxial tension) on two materials with very diverse mechanical and fracture properties – CR4 and DP800 steel. The comparisons are done for full-field strain contours, fracture strains and strain paths/triaxialities generated using the two DIC systems. A simple technique is proposed to compensate for the effects of out-of-plane motion in the 2D measurements. It is shown that 2D-DIC can capture the material deformation with sufficient accuracy not only for planar specimens but also for certain scenarios involving out-of-plane motion (like balanced biaxial tension) by theoretical compensation of the strains.

KEYWORDS

Digital Image Correlation, full-field strain, optical metrology, fracture strain, Advanced high-strength steel

1. INTRODUCTION

Digital Image Correlation (DIC) is a non-contact optical metrology technique that was introduced in the 1980s. However, the popularity and the usage of DIC for material characterization has tremendously increased in the past 15 years, in both academia and industry. The application of DIC in studying material deformation is manifold, including but not limited to mechanical testing (elastic-plastic behavior, fracture mechanics at quasi-static to high strain rates), low cycle fatigue, damage propagation, and component-level testing [1-5]. This work focuses particularly on the use of DIC in characterizing the fracture behavior of sheet metals. The most popular and advanced material damage-failure prediction models like the Generalized Incremental Stress State dependent damage Model (GISSMO) by Andrade et al. [6] need a fracture locus, that is obtained by various fracture loci interpolation models like the Xue-Wierzbicki model [7], Modified Mohr-Coulomb (MMC) model by Bai and Wierzbicki [8], and eMMC model by Jia and Bai [9]. All these advanced fracture models are calibrated based on the experimentally determined fracture strains, measured using multiple techniques [10] including DIC.

The simplest form of a DIC system used for measuring the fracture strains is a 2D-DIC system utilizing a single camera that captures the deformation in the material in a sequence of images, which are later processed using different DIC algorithms to generate the full-field strain history. Post-processing of the DIC strain maps helps in determining the localized fracture strains just before the initiation of crack. [10] Due to the nature of the technology, 2D-DIC is limited to in-plane deformations where the camera is kept normal to the deforming surface. Any out-of-plane translations and/or rotations can theoretically lead to inaccurate measurements. In this light, a stereo-DIC (3D-DIC) system proves advantageous over a 2D-DIC system by allowing a practical and powerful solution based on the principles of binocular stereo vision and digital image correlation for measuring large strains [11]. Nonetheless, stereo DIC has its limitations. In particular: (i) the two (or more) cameras in a stereo DIC must be strictly synchronized such that the images are captured at the same instant, or else significant errors will result especially in high-speed testing; (ii) The requirement of two cameras oriented at an angle sometimes limits the application due to spatial and environmental constraints in setups requiring high magnification [12]; (iii) the cost of stereo DIC is much higher as compared to 2D-DIC, especially for high-speed measurements. Because of these limitations associated with stereo DIC, 2D-DIC is still a popular choice for measuring the fracture strains in sheet specimens of Advanced High Strength Steels (AHSS) and aluminum alloys [13-16] to calibrate the fracture models for finite element analysis. However, the accuracy of prediction of these advanced fracture models is only as good as the experimental data fed to calibrate them. Therefore, it is crucial that the errors in these measurements are well understood and quantified to (i) estimate the errors in the collected data and (ii) determine whether the counted errors can be separated and removed from the actual measurements [17].

Over the years, researchers have proposed several solutions to minimize/compensate for the errors and improve the accuracy of 2D-DIC measurements. There have been several works by Sutton et al. [17], Pan et al. [18, 19] where the researchers showed that a 2D-DIC system with an object space or a bilateral telecentric lens can substantially improve the accuracy of the system by making it insensitive to out-of-plane motions and lens distortions. However, telecentric lenses are (i) heavy and bulky, (ii) limited in their field of view and depth of field, (iii) restricted to a fixed measuring distance and magnification, and (iv) 10 times as expensive as comparable standard lenses [18], which make them impractical for certain applications. There have been certain studies to theoretically determine the error due to out-of-plane translations and rotations [20-23] using a rigid non-deformable object with the tested sample and ex-situ removing the artificial strains from the measurements. Pan et al. [19], Bai et al. [20], and Wittevrongel et al. [22] tested the theoretical compensation of errors on small strains on a uniaxial tension sample. There are no studies that directly aim at quantifying the errors in measuring the comparatively large fracture strains for different loading conditions. In this paper, we evaluate the effectiveness of 2D DIC for mechanical tests intended to generate a fracture strain curve of sheet material.

The errors in a 2D-DIC measurement can be attributed to several factors. Zhao et al. [24] have categorized the error sources in DIC measurements into two categories: (i) errors due to the DIC analysis algorithm (shape function, correlation criteria, interpolation scheme, and subset size); (ii) errors due to the image acquisition process (speckle pattern, lens distortion, environmental noise, out-of-plane motion, calibration). In this work, we focus on the latter category of errors. The novelty of the work is the carefully designed set of experiments to evaluate the accuracy of the fracture strains recorded by 2D-DIC compared to a stereo DIC system for four loading paths contributing to a fracture strain curve. The study entails experimental work around the development of fracture strain curves for two important grades of steel – CR4, and DP800. The experiments are performed for the two grades of steel for four loading conditions: (i) uniaxial tension, (ii) plane strain, (iii) shear, and (iv) balanced biaxial tension. All the experiments are done using a specially designed setup simultaneously employing a high-resolution custom-built 2D-DIC and a commercial stereo DIC. The captured images are processed using the same DIC algorithm and process parameters, to isolate the errors in 2D-DIC measurements (keeping stereo DIC as the benchmark), especially those induced due to the out-of-plane motion, lens distortion, and calibration.

2. EXPERIMENTAL TECHNIQUES

2.1. Materials and Specimens

The experiments are performed on 0.75 mm thick CR4 steel sheets and 1.5 mm thick DP800 steel sheets. The quasi-static stress-strain curves and baseline tensile properties of the two target materials in the rolling direction are shown in Figure 1 and Table 1. The two chosen materials represent two extremes in terms of mechanical properties. CR4 is an automotive outer-body material with relatively low strength and high ductility, while DP800 is a structural material with higher strength and lower ductility.

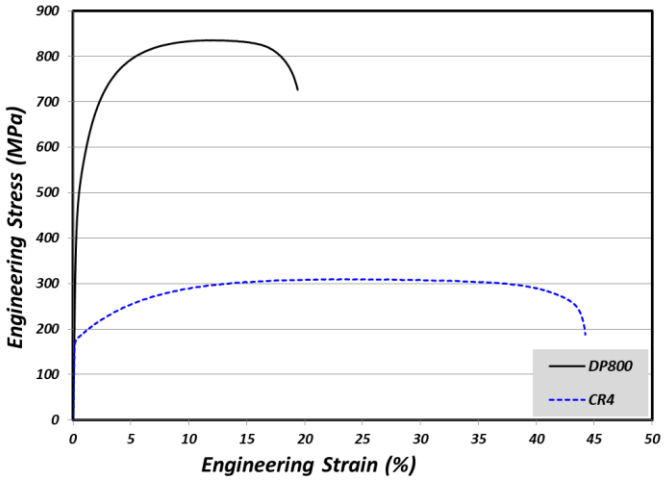

Figure 1: Uniaxial tension stress-strain curves of CR4 and DP800 steel

Four different types of specimen geometries (as shown in Figure 2) are extracted from the two materials. Each geometry pertains to a certain strain path or triaxiality (refer to Appendix A.1) on the fracture strain curve. The fracture strains extracted from these geometries are plotted against the true triaxiality of that specimen geometry, which is fit to a fracture model, as shown in Figure 2. The details of specimen geometries tested in this work are given below.

- Uniaxial Tension (UT) specimens (ideal triaxiality 0.333): The UT specimens (based on ISO 6892-1) feature a 12.5 mm wide and 70 mm long gauge section.
- Notched tensile specimens for Plane Strain Tension condition (PST) (ideal triaxiality 0.577): The notched tensile specimens have a 20 mm wide gauge region with circular cutouts of radius 5 mm, reducing the width of the gauge region to 10 mm in the center.
- Shear specimens (SH) (ideal triaxiality 0.0): The shear specimens are based on a custom geometry.
- Balanced Biaxial Tension (BBT) specimens (ideal triaxiality 0.667): The BBT tests are run on flat square sheets of side 180 mm.

UT and PST specimens are extracted using waterjet cutting, SH specimens are produced using wire-cut EDM, and BBT specimens are cut on a hydraulic shear. All the specimens are prepared such that the rolling direction is along the tensile axis of the specimen (this does not apply to BBT specimens).
Before testing, a random speckle pattern is applied to the surface of the specimens facing the cameras as shown in Figure 5. Three specimen repeats per geometry are tested to evaluate the repeatability of the results.

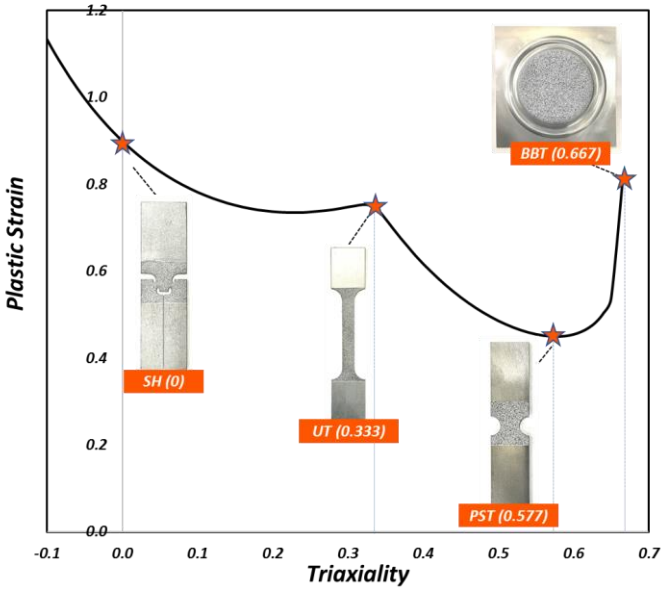

Figure 2: A representative curve of fracture strain vs. triaxiality with specimen geometries tested to generate the required triaxialities

2.2. Experimental Setup

2.2.1. Experimental Setup for UT, PST, and SH

The tests are conducted on a ZwickRoell Z050 electromechanical load frame with hydraulic grips and a 50 kN load cell. The setup (shown in Figure 3) includes two DIC systems recording the deformation simultaneously. The 2D-DIC has custom hardware utilizing a Basler 16.1 megapixel CMOS camera that is oriented to view the specimen normally, while the stereo DIC is a GOM ARAMIS 12 megapixel system. The choice of optics for the setup is done to ensure similar pixel densities (microns/pixel) for the 2D-DIC and stereo DIC. All the experiments are performed at quasi-static speeds with an average strain rate of 0.005 s^{-1}. The optical system parameters for UT, PST, SH, and BBT tests are given together in Table 2.

Table 1: Mechanical Properties of CR4 and DP800 steel

Material	Thickness (mm)	0.2% Offset Yield Strength (MPa)	Ultimate Tensile Strength (MPa)	Uniform Elongation (%)	Total Elongation (%)
CR4	0.77 ± 0.02	177.2 ± 0.7	307.6 ± 1.8	23.3 ± 2.0	43.0 ± 1.2
DP800	1.50±0.01	557.3 ± 8.4	834.3 ± 5.9	11.8 ± 0.6	19.3 ± 0.2

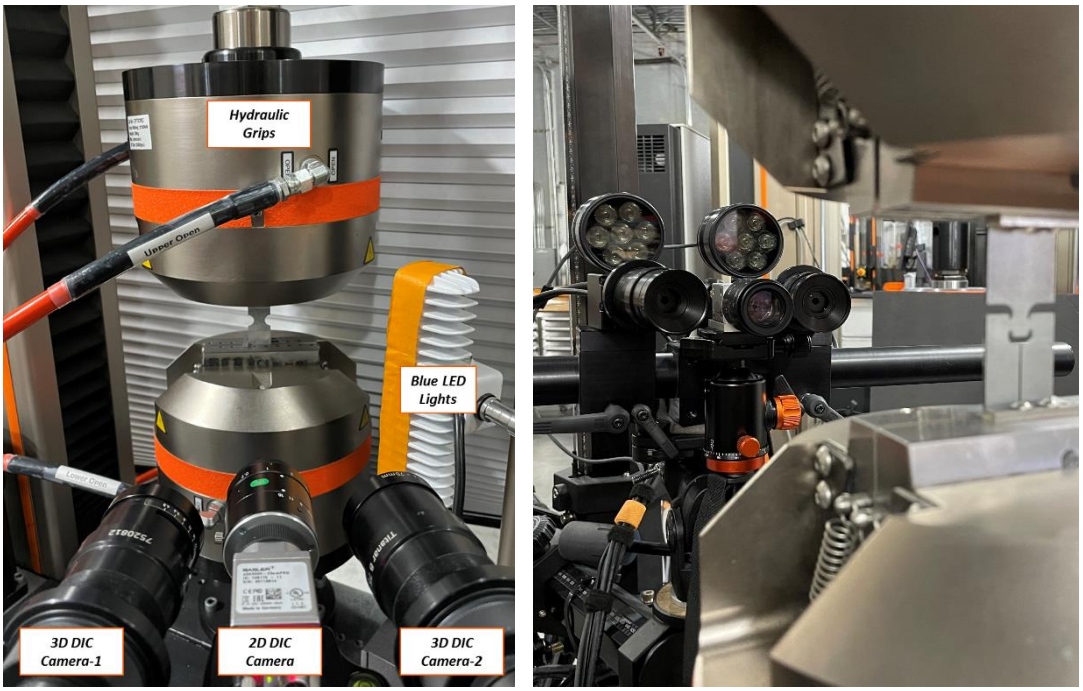

Figure 3: Test setup for planar specimens (UT, PST, and SH) on load frame showing 2D-DIC and stereo DIC cameras capturing the sample deformation simultaneously

Table 2: Optical System Details and DIC Processing Parameters

	UT		PST and SH		BBT	
	Stereo DIC	**2D-DIC**	**Stereo DIC**	**2D-DIC**	**Stereo DIC**	**2D-DIC**
Camera	GOM ARAMIS 12 MP	Basler 16 MP	GOM ARAMIS 12 MP	Basler 16 MP	GOM ARAMIS 6 MP	Basler 8 MP
Lenses	Schneider Xenoplan 50 mm	Computar 50 mm	Rogonar-S Titanar B 75 mm	Computar 50 mm	Schneider Xenoplan 50 mm	Basler 25mm
Lighting	Blue LED	Blue LED	Blue LED	Blue LED	Blue LED	Blue LED
Frame Rate (Hz)	20	20	10	10	20	20
Resolution (pixels x pixels)	4096x3000	5328x3032	4096x3000	5328x3032	2752x2200	2840x2840
Measuring Distance Z (mm)	500	650	350	300	550	450
Pixel Resolution (microns/pixel)	34	31	12	12	45	49
Facet Size (pixels)	45x45	45x45	65x65	65x65	43x43	43x43
Point Distance (pixels)	15	17	21	21	12	11
Virtual Gauge Length (mm)	~1.02	~1.05	~0.50	~0.50	~1.08	~1.08
Interpolation	Bicubic	Bicubic	Bicubic	Bicubic	Bicubic	Bicubic
Facet Matching	Against Ref. Stage	Against Ref. Stage	Against Ref. Stage	Against Ref. Stage	Against Ref. Stage	Against Ref. Stage
Software	GOM Correlate	GOM Correlate	GOM Correlate	GOM Correlate	GOM Correlate	GOM Correlate

2.2.2. Experimental Setup for BBT

The balanced biaxial tests are performed on a custom-built Interlaken SP400 servo-hydraulic press with a capacity of 2000 kN. The top of the press has a circular opening which allows the DIC cameras to view the specimen during deformation. The 2D-DIC and stereo DIC cameras are mounted on the top of the press as shown in Figure 4. The 2D-DIC has custom hardware utilizing a Basler 8 megapixel CMOS camera that is set up to view the specimen normally, while the stereo DIC is a GOM ARAMIS 6 megapixel system (Refer to Table 2 for details). The tests are conducted based on the Marciniak testing approach where a square specimen is clamped on all the sides with a clamping load of 1000kN, while a cylindrical punch (with a diameter of four inches and a flat top) deformed the specimen at 0.5 mm/s. The Marciniak tests are well known in the industry for Formability Limiting Curve (FLC) determination and the details of the test can be referred to in the work by Hu [25].

Finally, the two camera systems were programmed to auto-trigger at the start of the test. This was done using a digital input from the Zwick load frame (for UT, PST, and SH) and the ITC SP400 hydraulic press (in case of BBT) which triggered the two camera systems simultaneously.

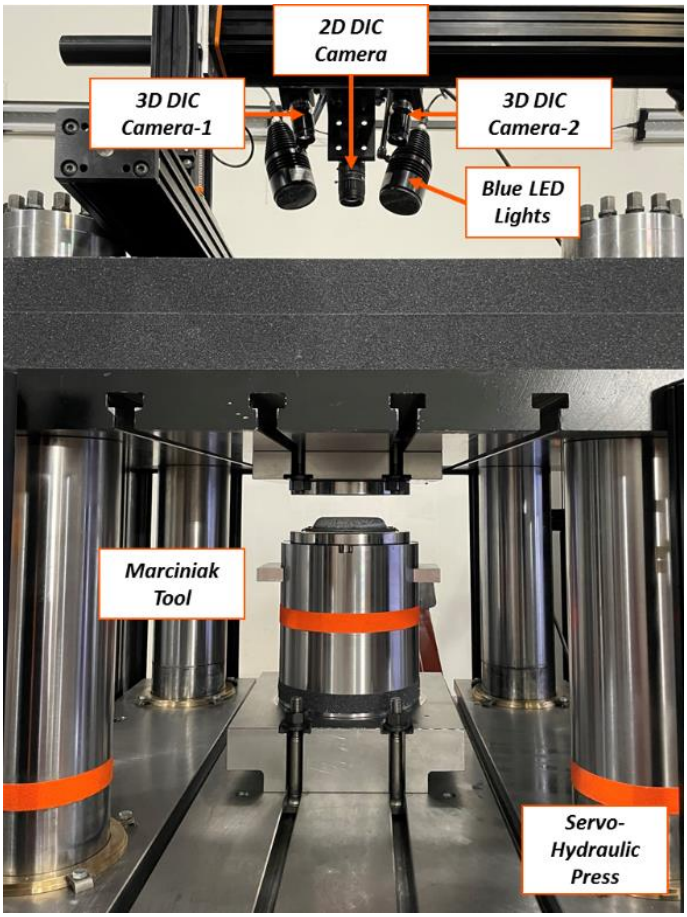

Figure 4: Test setup for BBT specimens on a servo-hydraulic press showing roof-mounted 2D-DIC and stereo DIC cameras

2.3. DIC Calibration

The calibration of the GOM ARAMIS stereo DIC system uses camera views of a standard calibration panel in 13 different orientations. Using the images, the system locks in the position of the left and the right cameras and determines the intrinsic parameters (like camera angle, calibration deviation, stereo residual, camera angle, etc.). For all the tests, it is ensured that the stereo DIC system is freshly calibrated and has a calibration deviation of less than 0.05 pixels.

The calibration of the 2D-DIC system is based on an image with a ruler held at the same measuring distance as the specimen, as shown in Figure 5.

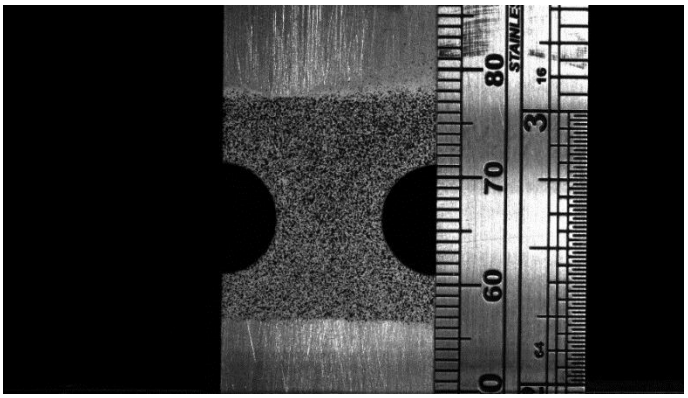

Figure 5: PST specimen painted with a speckle pattern; and a graded ruler used for the calibration of the 2D-DIC system showing 3000 pixels in the Y direction covering 36 mm length (12 microns/pixel).

2.4. Acquisition Parameters

Several important parameters were carefully selected to have a fair comparison between the two DIC systems.

Pixel Resolution: The pixel resolution (measured in microns per pixel) in DIC measurement is the connection between the actual physical length and the number of pixels representing it. The camera optics and the measuring distance of the two DIC systems were carefully selected to obtain the same pixel resolution for each test geometry. The details of the camera setup are given in Table 2.

Camera Frame rate: It is believed that the fracture strain measured by an imaging system is dependent on the camera acquisition rate. A faster camera acquisition rate is required to capture the last image before the fracture as close as possible to the moment of fracture. Contrary to this opinion, Hu et al. [10] compared the fracture strain results obtained at different frame rates (1fps, 10 fps, 100fps, and 500 fps) and found that the measured fracture strain values did not increase with the increase in camera frame rate. Despite this observation, the camera frame rate must be sufficiently high to capture the fracture strains. Furthermore, this work aims to compare the fracture strains recorded by the two DIC systems. For this purpose, the same camera rate is used for both the DIC systems, as mentioned in Table 2.

Virtual Strain Gauge Length (VSGL): The most important parameter for DIC result comparison is the virtual strain gauge length used for strain computation. The facet sizes and point distances used for DIC processing of the 2D-DIC and stereo DIC files were selected to obtain the same virtual strain gauge length. The complete list of parameters used for DIC processing of each geometry is given in Table 2.

2.5. Post-Processing and Extraction of Fracture Strains

The sets of images captured by the two DIC systems are processed using the same commercial DIC software - GOM Correlate Professional. It was made sure that the stereo DIC was appropriately calibrated with a maximum allowed intersection deviation of 0.5 pixels to be able to use a benchmark for comparison.

On the last stage before fracture, the point of maximum effective strain is chosen, and designated as the 'Fracture Point'. Finally, the fracture strains are obtained over 0.5 mm long virtual extensometers in the X and Y directions across the 'Fracture Point'. The extracted results are presented in the next section.

3. EXPERIMENTAL RESULTS

3.1. Uniaxial Tension (UT) Tests

To check the validity of the results obtained from the two DIC systems, the full-field major strain maps for CR4 (Figure 6) and DP800 (Figure 7) and the engineering stress-strain curves (Figure 8) from the two systems are compared. Strain is calculated over a 50 mm long virtual extensometer drawn in the center of the sample as shown in Figure 6 and Figure 7. The stress-strain curves show an excellent match in total ductility for both materials. Therefore, the two DIC systems capture the overall stress-strain behavior of the material without much disparity in the results.

For CR4, the average effective true strain from stereo DIC is 0.975 ± 0.008, while the average effective true strain for 2D-DIC is 0.886 ± 0.004. On the other hand, the average effective true strain for DP800 calculated by stereo DIC is 0.543 ± 0.022 as compared to 0.546 ± 0.014 for 2D-DIC. The von Mises effective fracture strains for CR4 differ by 10% for the two DIC systems, while the fracture strain values for DP800 are statistically the same. The strain contour map shows that the CR4 sample undergoes much more severe localized necking before fracture as compared to the DP800 UT sample. The differences in the fracture strains captured by the two DIC systems vary for large strain values in the case of CR4, while they are captured well for smaller fracture strain values (DP800).

A detailed summary showing the fracture strains from the two DIC systems for each sample is available in Appendix Table A1 and Table A2.

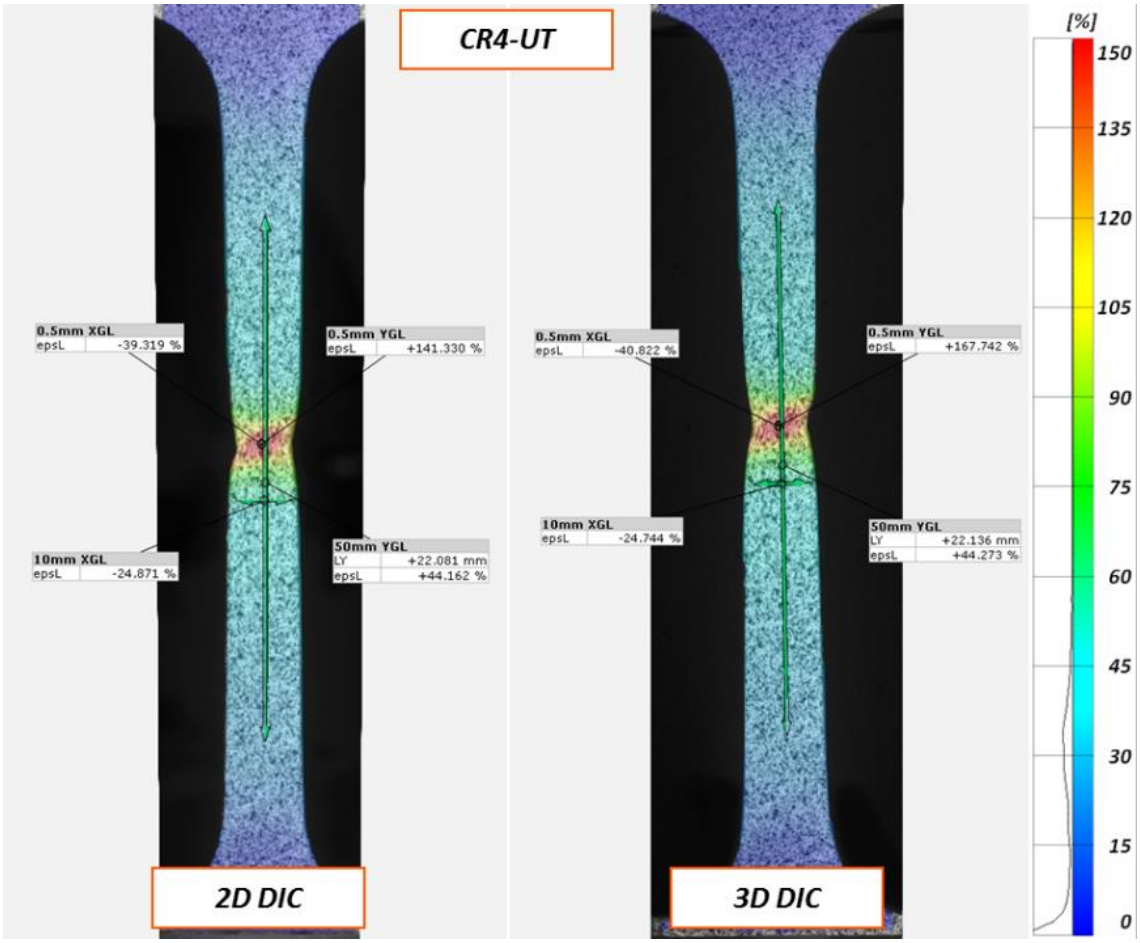

Figure 6: Comparison of major strain (engineering) contour for 2D-DIC and stereo DIC for UT test of CR4 steel

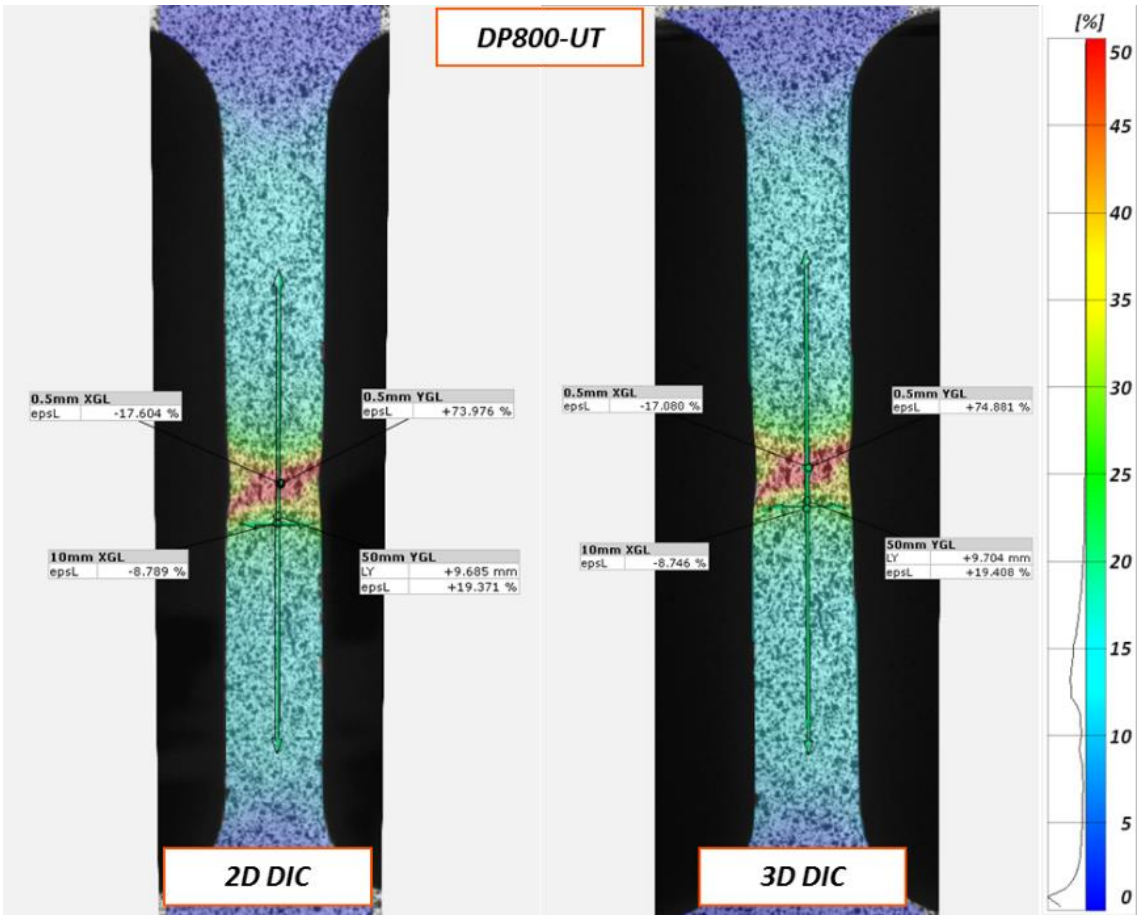

Figure 7: Comparison of major strain (engineering) contour for 2D-DIC and stereo DIC for UT test of DP800 steel

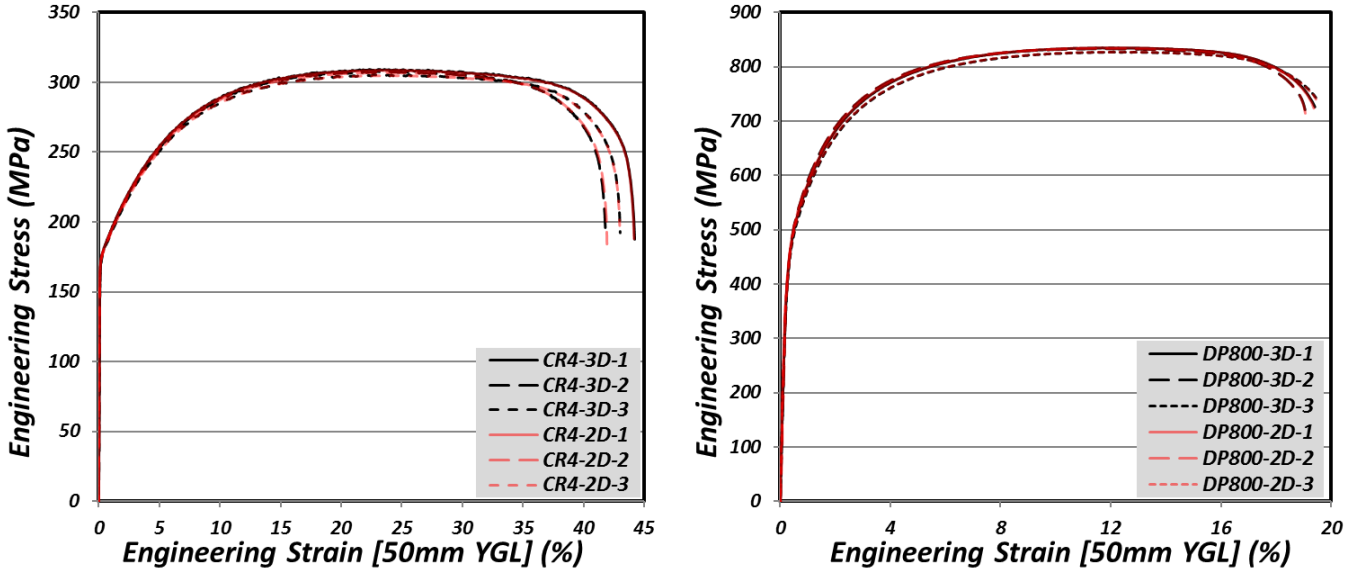

Figure 8: Comparison of engineering stress-strain curves for 2D-DIC and stereo DIC for UT test of CR4 (left) and DP800 (right) steel

3.2. Plane Strain Tension (PST) Tests

First, the validity of the results is checked on the global level by comparing the displacement over a 12 mm long virtual extensometer drawn on the sample across the notch. Second, the full-field major strain map for CR4 (Figure 9) and DP800 (Figure 10) from the two DIC systems are compared. The 12mm Y-displacement and the full-field major strain contour are similar and the two DIC systems capture the strain distribution on the samples very well.

The average effective true strain for CR4 for stereo DIC is 0.768 ± 0.004 while it is 0.764 ± 0.004 for the 2D-DIC system. The average effective true strain for DP800 for stereo DIC is 0.441

± 0.01 while it is 0.433 ± 0.018 for the 2D-DIC system. The fracture strains recorded by the two DIC systems are within the statistical limits, and the 2D-DIC can record the PST fracture strains well for both materials.

The average triaxiality at fracture for DP800 samples is 0.55 whereas for CR4 the average triaxiality at fracture is 0.49. Hence, the DP800 notched sample has a better plane strain fracture as compared to the CR4 sample.

A detailed summary showing the fracture strains from the two DIC systems for each sample is available in Appendix Table A3 and Table A4.

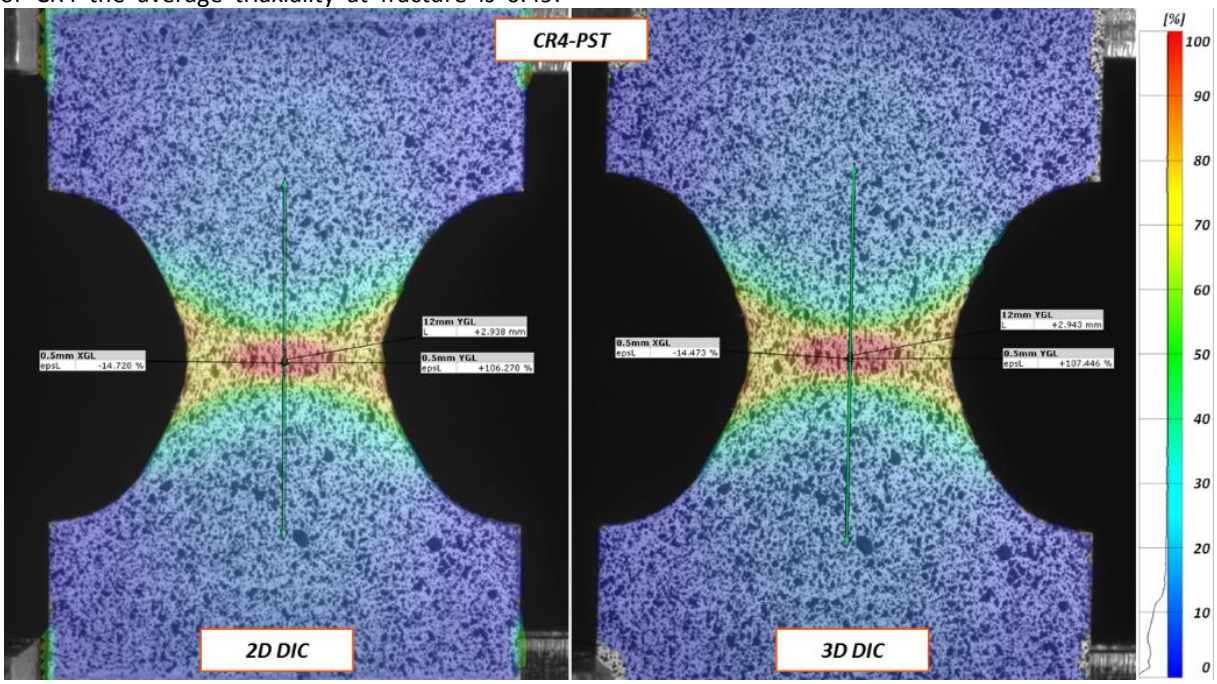

Figure 9: Comparison of major strain (engineering) contour for 2D-DIC and stereo DIC for PST test of CR4 steel

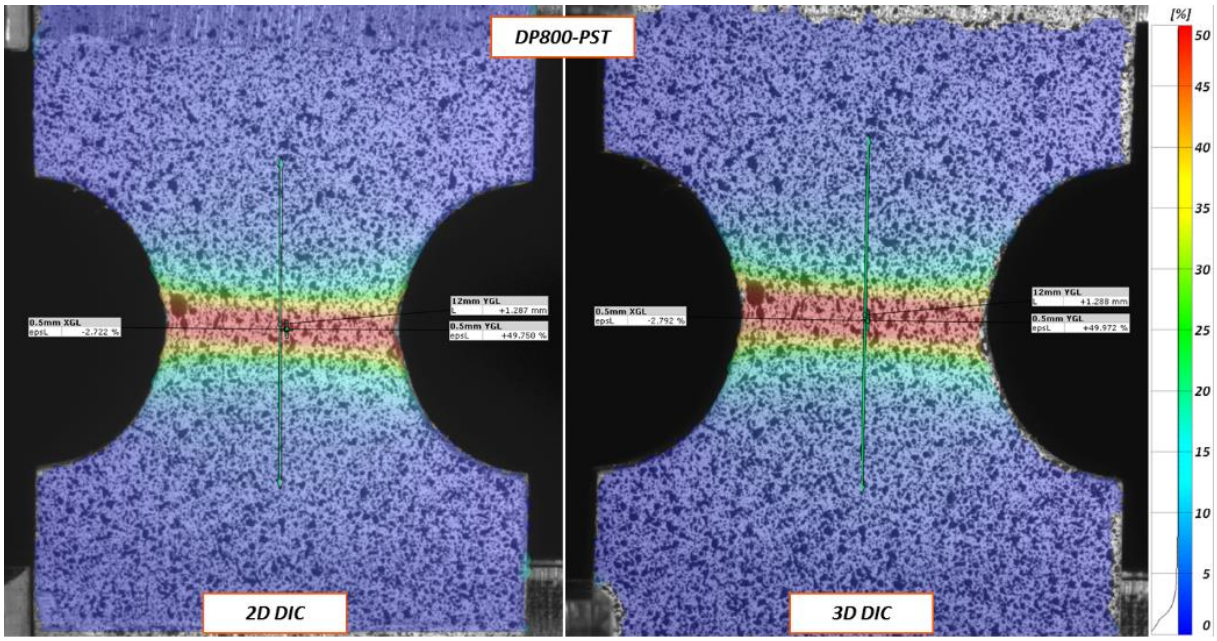

Figure 10: Comparison of major strain (engineering) contour for 2D-DIC and stereo DIC for PST test of DP800 steel

3.3. Shear (SH) Tests

Figure 11 and Figure 12 present the full-field major strain maps from the 2D-DIC and stereo DIC systems for CR4 and DP800 steels respectively. As with the PST samples, the results are first compared on a global level. The displacement on a 15 mm extensometer for the left and the right leg of the specimen are compared within each sample for any misalignment while testing, then the displacement values for the 2D-DIC and stereo DIC are compared along with the full field shear strain

contours. The two DIC systems perform very similarly on a global strain level.

For CR4, the average fracture strain for stereo DIC is 1.104 ± 0.032 while the same for 2D-DIC is 1.110 ± 0.014. The average fracture strain value for DP800 for stereo DIC is 0.659 ± 0.021 while the same for 2D-DIC is 0.645 ± 0.016. The strain values for the two materials from 2D-DIC and stereo DIC are well within the experimental scatter of the two materials.

The average triaxiality at fracture for CR4 samples is 0.125 whereas for DP800 the triaxiality at fracture is 0.070, which are both very close to the ideal shear triaxiality of 0.

A detailed summary showing the fracture strains from the two DIC systems for each sample is available in Appendix Table A5 and Table A6.

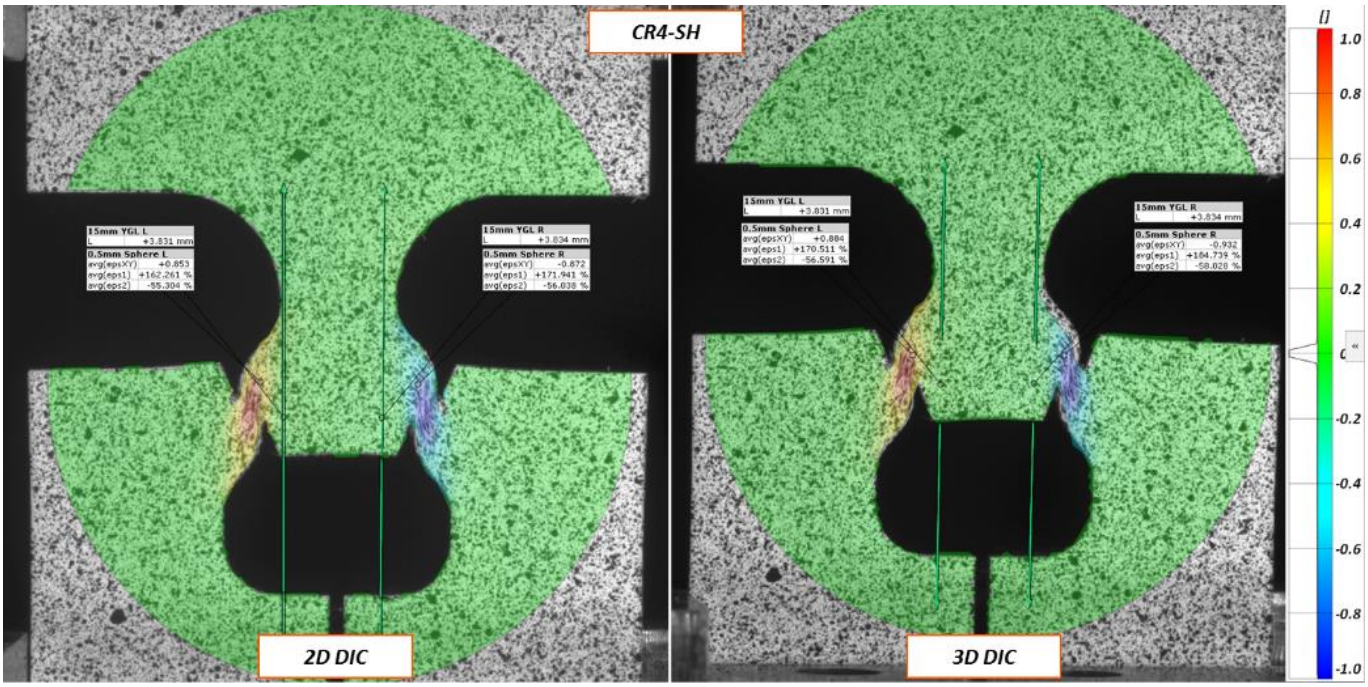

Figure 11: Comparison of shear strain (true) contour for 2D-DIC and stereo DIC for SH test of CR4 steel

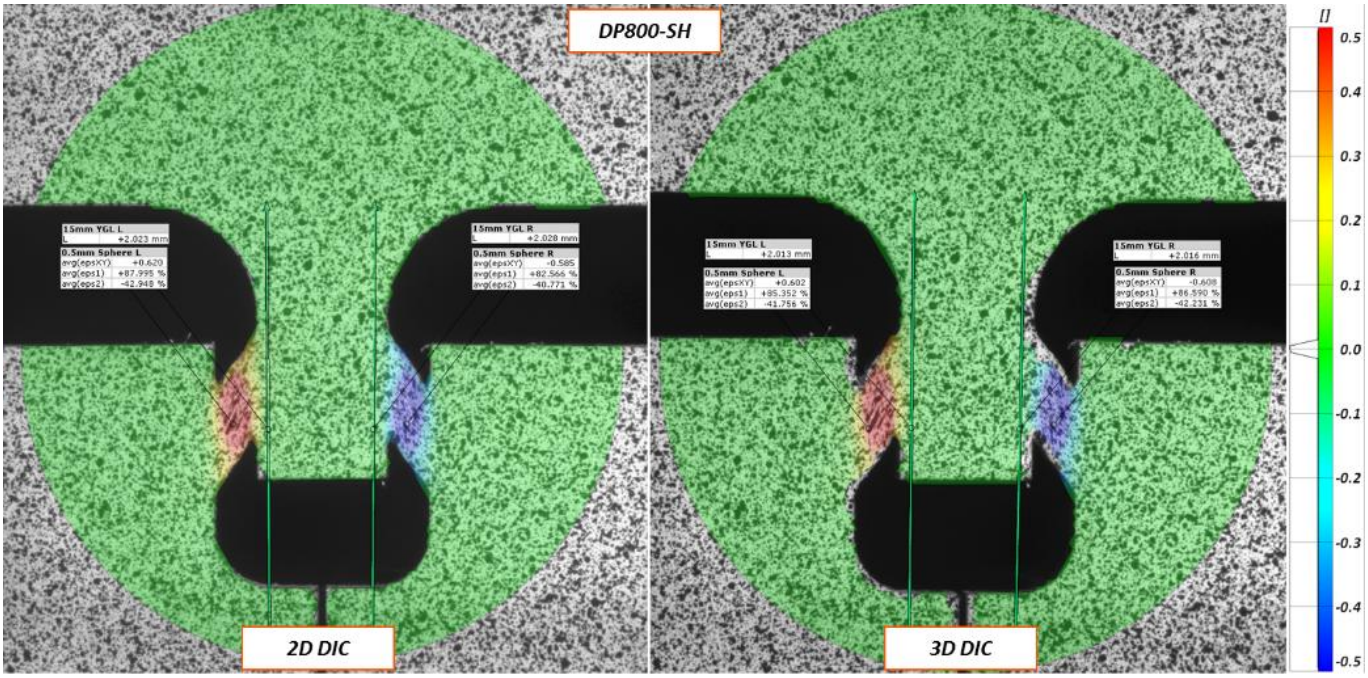

Figure 12: Comparison of shear strain (true) contour for 2D-DIC and stereo DIC for SH test of DP800 steel

3.4. Balanced Biaxial Tension (BBT) Tests

The full-field major strain maps from the 2D-DIC and stereo DIC systems for CR4 and DP800 steels for Marciniak tests are extracted and compared. There is a considerable difference in the 2D-DIC and stereo DIC major strain full-field strain contours for both materials. Upon closer evaluation, the full-field strain contours are found similar if the legends are offset by a certain value. It is seen that the strain levels for 2D-DIC are scaled up, as compared to the strains computed by the stereo DIC. Figure 14 and Figure 15 show the major strain maps of the two materials with different legends for 2D-DIC and stereo DIC results.

For CR4, the average effective true fracture strain for stereo DIC is 0.758 ± 0.077 while the fracture strain for 2D-DIC is 0.860 ± 0.061. For DP800, the average effective true fracture strain for stereo DIC is 0.439 ± 0.027 while the fracture strain for 2D-DIC is 0.527 ± 0.029. Like the major strain contours, there is a considerable difference in the 2D-DIC and stereo DIC fracture strains and the major strain full-field strain contours for both the materials.

The average triaxiality at fracture for both CR4 and DP800 steel samples is 0.667, which is ideal for a balanced biaxial condition.

Out-of-plane error compensation: During a Marciniak test, the test sample deforms and grows out of the initial calibrated plane. As a result, the measuring distance between the deformed test sample and the 2D-DIC (as well as the stereo DIC) camera decreases, which leads to out-of-plane error in 2D measurements. The Marciniak test sample moves closer to the camera, but the entire deformation zone moves in the sample plane like an inverted cup, unlike in the case of Nakajima testing where the deformation is in the shape of a hemispherical dome [25]. This means that the error in the 2D-DIC measurements for Marciniak tests is systematic that is added equally to all the points in the deformation plane.

This out-of-plane deformation in the sample leads to a strain increase in the sample. Figure 13(a) shows a schematic of the Marciniak test with a single camera system. Figure 13(b) shows a ray diagram for the single-camera system. It is theoretically derived that the strain error added to the measurement due to out-of-plane motion is equal to the ratio of change in measuring distance and the initial measuring distance ($\Delta z/z$), also suggested by Sutton et al. [12]. The out-of-plane error can be removed from the recorded measurement using eq. (1).

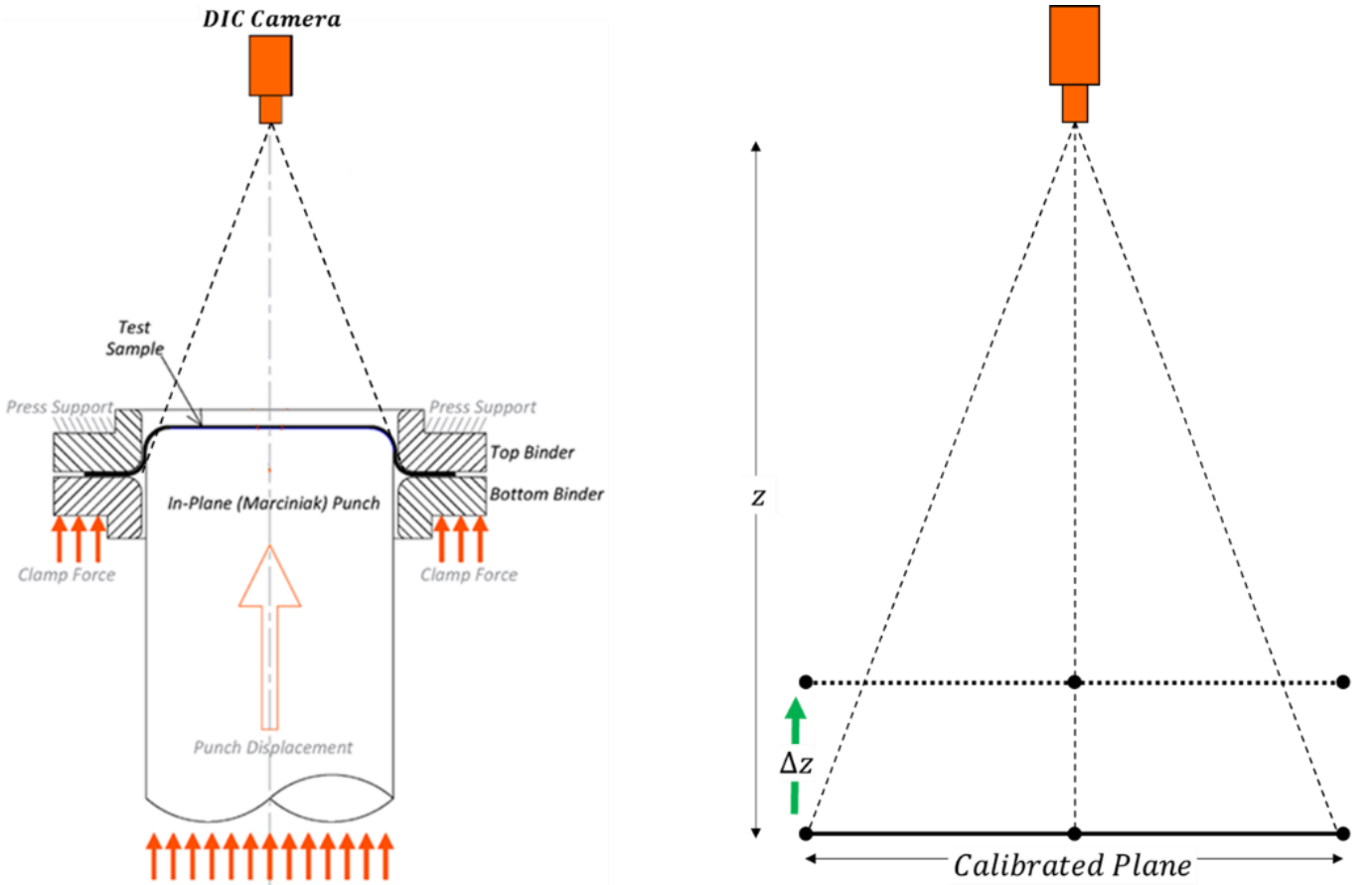

Figure 13: (a) Schematic showing Marciniak test setup using a 2D-DIC and (b) Out-of-plane translation from material deformation at the camera sensor plane for a standard single-camera system

$$Strain(\%)_{compensated} = Strain\ (\%)_{measured} - \frac{\Delta z}{z}(\%) \quad (1)$$

$$Cup\ Height\ \Delta z = Punch\ Speed\ x\ Test\ Time \quad (2)$$

The out-of-plane displacement in a Marciniak test is the cup height, which is calculated using eq. (2). The punch speed of the Marciniak BBT test (0.50 mm/s) is multiplied by the test time to calculate the cup height (Δz). Since the 2D-DIC camera is calibrated for an initial measuring distance (z) of 450 mm (given in Table 2), the artificial strain ($\Delta z/z$) in the measurements, caused only due to the out-of-plane motion can be calculated for each time step and subtracted from the measurements.

The out-of-plane compensated effective true fracture strain for 2D-DIC for CR4 is 0.776 ± 0.061 while the compensated effective fracture true strain for DP800 is 0.444 ± 0.028. The compensated values for 2D-DIC are in close agreement with the stereo DIC values, and well within the statistical limits. This shows that the out-of-plane motion error, in this case, is a case of systematic error that can easily be separated and removed from the recorded strain to generate the actual strain.

A detailed summary showing the fracture strains from the two DIC systems for each sample is available in Appendix Table A7 and Table A8.

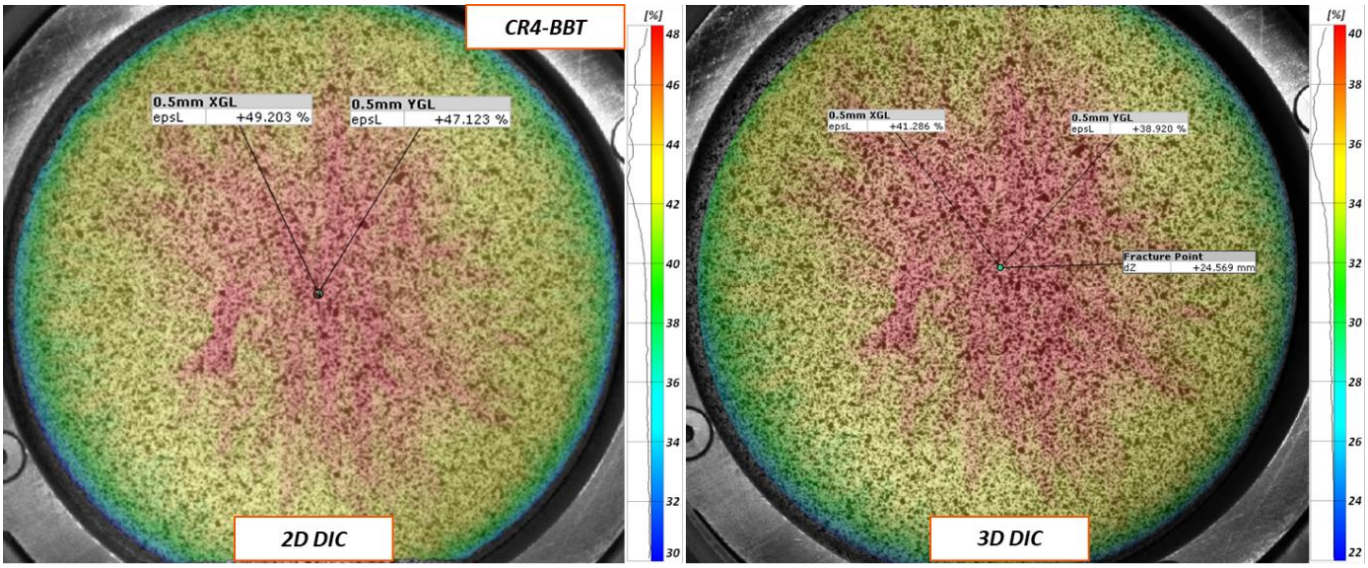

Figure 14: Comparison of major strain (engineering) contour for 2D-DIC and stereo DIC for BBT test of CR4 steel. Note that the legend for stereo DIC is 22%-40% while for 2D-DIC is 30%-48%.

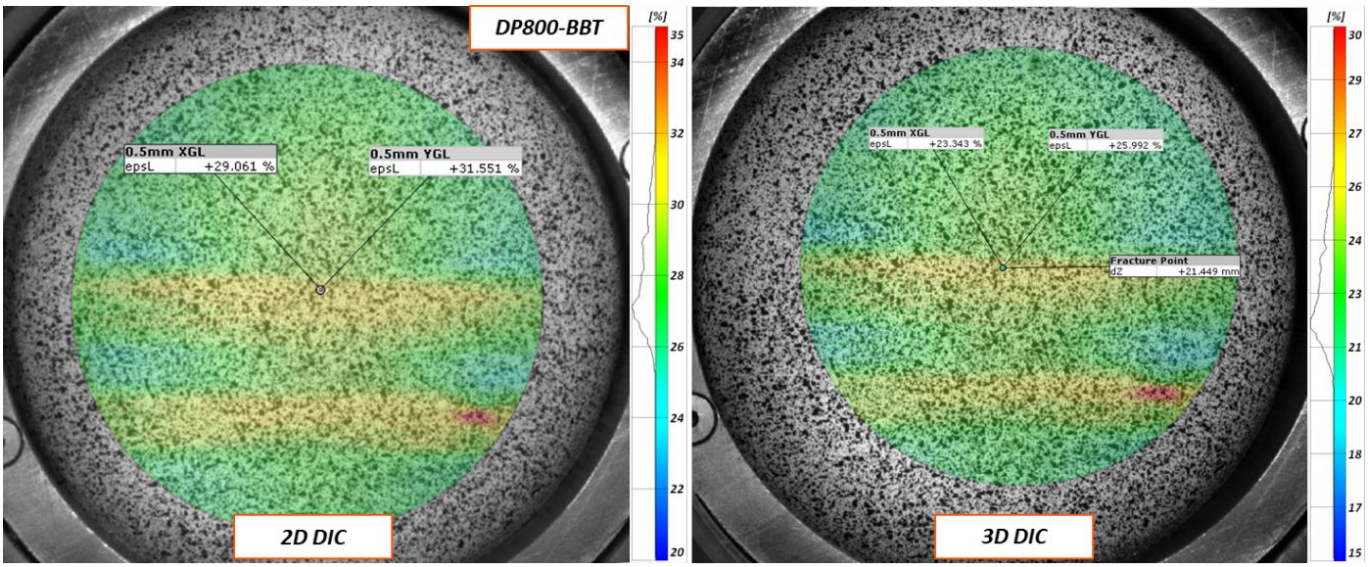

Figure 15: Comparison of major strain (engineering) contour for 2D-DIC and stereo DIC for BBT test of DP800 steel. Note that the legend for stereo DIC is 15%-30% while for 2D-DIC is 20%-35%.

4. DISCUSSION

The images acquired by the two DIC systems are processed using the same DIC software, hence there is no effect of the DIC algorithm on the results obtained from the two DIC systems. The two systems are used to simultaneously capture the deformation in the same specimen, thereby eliminating the effect of the speckle pattern in the comparison. The errors in the results between the 2D-DIC and stereo DIC are solely due to the acquisition process– camera optics, calibration procedure, and out-of-plane motions/rotations.

As expected from the grade of steel, the two materials exhibit very different fracture behavior. The strain paths (major strain vs. minor strain, like a formability limiting curve or FLC) for the two materials (given in Figure 16) show that the same specimen geometries perform differently for the grades of steel. The strain paths for DP800 are relatively linear, while those for CR4 show a high level of nonlinearity which increases with the magnitude of strain. The nonlinear nature of the loading path is more clearly presented in the fracture strain vs. triaxiality curve (Figure 17). The triaxialities at fracture for all the geometries (except for UT specimens) are closer to the ideal values for the stronger and less ductile DP800, as compared to CR4.

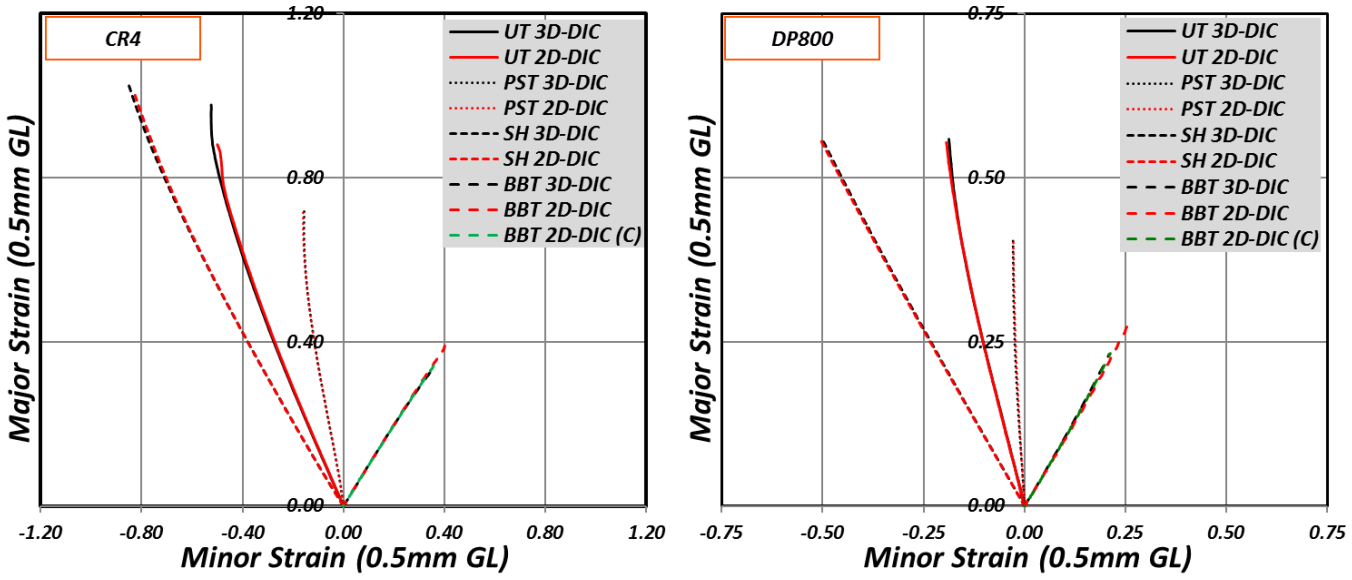

Figure 16: Comparison of strain path for the four tested geometries for CR4 and DP800 for 2D-DIC, stereo DIC and out-of-plane compensated 2D-DIC

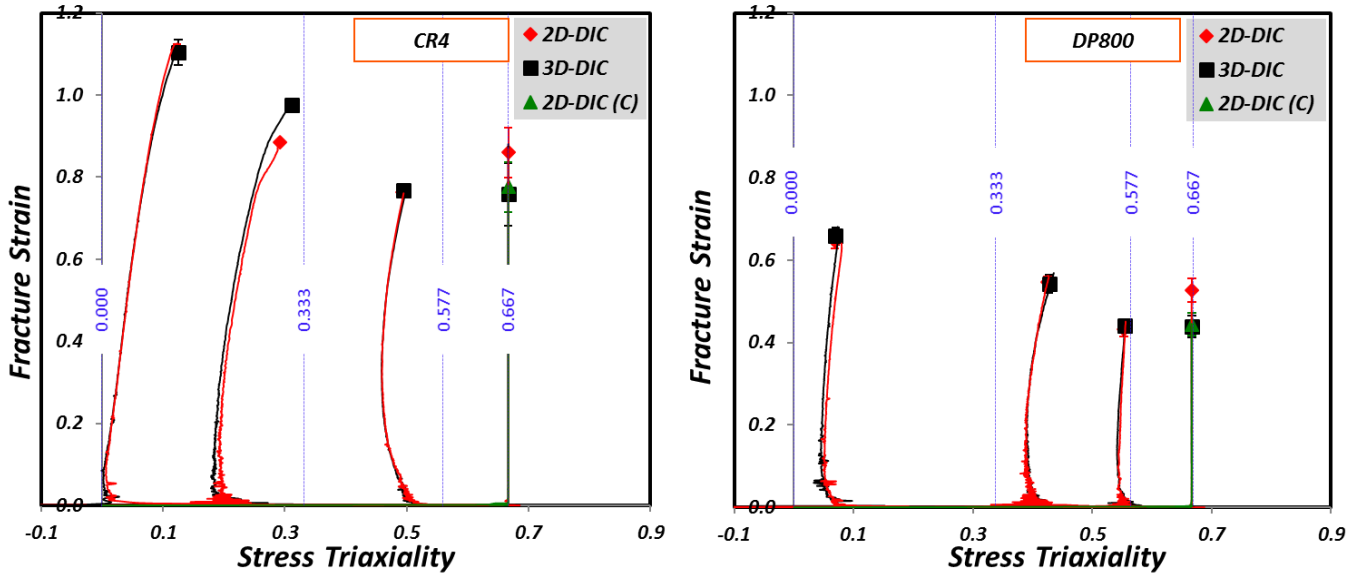

Figure 17: Fracture strain vs. triaxiality curve for the four tested geometries for CR4 and DP800 for 2D-DIC, stereo DIC, and out-of-plane compensated 2D-DIC (C)

The 2D-DIC captures the strain path in both materials well. However, there are some disparities in the fracture strains:

- The 2D-DIC system captures the fracture strains in the planar samples (UT, PST, SH) for DP800 at an acceptable level. However, there is a 10% difference in the fracture strains measured for the UT specimens of the more ductile CR4 steel. This suggests that 2D-DIC is an acceptable choice for measuring the fracture strains, especially for medium-ductile materials, while some errors are incurred in the measurements in the case of materials that exhibit strong localized necking (large fracture strains).
- There are significant errors in the 2D-DIC measurements for the BBT tests due to the out-of-plane motion in the samples. It is confirmed that the out-of-plane error in the 2D-DIC measurements for Marciniak tests can be theoretically predicted and compensated to achieve a closer match to the stereo DIC measurements. This shows that, against the general notion about 2D-DIC, a 2D-DIC system with a standard lens can produce reliable results for measuring the fracture strains even for out-of-plane cases like Marciniak tests. Also, the error in the out-of-plane measurements can be minimized by increasing the initial measuring distance (z).
- It is important to note that the specimens in the planar tests (UT, PST, SH) thin down during the plastic deformation and lead to some out-of-plane errors in the fracture zone. However, the magnitude of errors is negligible due to the magnitude of out-of-plane displacement induced by local thinning in the thin sheet samples. For example, a thinning reduction of 50% in the fracture zone for a 1mm thick sheet sample would result in an out-of-plane displacement Δz of 0.5 mm leading to an error of <0.001 strains (measured on a 450mm calibrated distance). Therefore, the errors in planar tests are not noticeable.

5. CONCLUSION

This work evaluates the effectiveness of 2D-DIC in a demanding and high-accuracy application by benchmarking the 2D-DIC strain measurements against a stereo DIC system. A series of mechanical tests on a variety of specimen geometries (UT, PST, SH, and BBT, intended for generating different strain paths for fracture study) are performed on two diverse materials – CR4 and DP800 steel. The tests are performed on a special setup that enables simultaneous strain measurements by a 2D-DIC and a stereo DIC system. It is ensured that the DIC files are processed using similar process parameters. Comparisons are made between the full-field strain contour maps, the fracture strains, and the strain paths/triaxialities captured by the two DIC systems.

The fracture strains captured by the 2D-DIC are in close agreement with the stereo DIC results for the plane strain and shear conditions for both the materials. However, the uniaxial tension results vary for the CR4 steel owing to its severe localized necking. The experimental results for the in-plane geometries (UT, PST, and SH) show that the 2D-DIC produces satisfactory results for all the loading conditions for a high-strength, low ductility DP800 steel, but the results vary by 10% for the uniaxial tension condition for a low-strength, high-ductility CR4 steel.

The full-field strain contours of the balanced biaxial tension Marciniak tests show that the 2D-DIC results are similar to the stereo DIC results if they are offset in the positive direction by a certain value. This shows that the out-of-plane errors in the 2D-DIC strains are systematic errors that can be separated and removed from the measurements. Based on this information, a simple compensation technique is proposed and validated to adjust the theoretically known out-of-plane errors in a balanced biaxial Marciniak test. The compensated 2D-DIC fracture strains match the stereo DIC results very well. Finally, it is concluded that the 2D-DIC is capable of generating satisfactory fracture strain curves (for all four strain paths) for sheet metals, with high accuracy, especially for materials like DP800 steel with relatively low localized necking and within 10% for high ductility materials like CR4 steel.

The future works can be focused on the formability testing and generation of a formability limiting curve (FLC) for sheet metal alloys using a 2D-DIC system using Marciniak and Nakajima testing.

DECLARATION OF COMPETING INTERESTS

The authors declare that they have no known competing financial interests or personal relationships that could have appeared to influence the work reported in this paper.

APPENDIX A

EXPERIMENTAL DATA – DIC GENERATED FRACTURE STRAINS IN TABULAR FORM

A.1. Stress Triaxiality

Stress Triaxiality is the degree of hydrostatic stress in a given stress state. In terms of von Mises effective stress, stress triaxiality (η) is a ratio of hydrostatic stress and von Mises effective stress [25].

It can also be expressed in the following form:

$$\eta = \frac{S+1}{\sqrt{3(S^2+S+1)}}$$

where S is the strain ratio defined by, $S = \frac{\varepsilon_{Major}}{\varepsilon_{Minor}}$

Table A1: Fracture strains obtained from 2D-DIC and stereo DIC (3D) for UT tests for CR4 steel								
Property	***Major Strain*** ε_{Major}		***Minor Strain*** ε_{Minor}		***Effective Strain*** $\varepsilon_{Effective\ von\ Mises}$		***Stress Triaxiality***	
Sample	***3D-DIC***	***2D-DIC***	***3D-DIC***	***2D-DIC***	***3D-DIC***	***2D-DIC***	***3D-DIC***	***2D-DIC***
CR4-UT-1	*0.978*	*0.881*	*-0.525*	*-0.500*	*0.979*	*0.884*	*0.310*	*0.291*
CR4-UT-2	*0.965*	*0.883*	*-0.525*	*-0.474*	*0.966*	*0.884*	*0.312*	*0.303*
CR4-UT-3	*0.980*	*0.887*	*-0.531*	*-0.510*	*0.981*	*0.890*	*0.315*	*0.281*
Avg.	***0.974***	***0.884***	***-0.527***	***-0.494***	***0.975***	***0.886***	***0.312***	***0.292***
Std. Dev.	***0.008***	***0.003***	***0.003***	***0.018***	***0.008***	***0.004***	***0.003***	***0.011***

Table A2: Fracture strains obtained from 2D-DIC and stereo DIC (3D) for UT tests for DP800 steel								
Property	***Major Strain*** ε_{Major}		***Minor Strain*** ε_{Minor}		***Effective Strain*** $\varepsilon_{Effective\ von\ Mises}$		***Stress Triaxiality***	
Sample	***3D-DIC***	***2D-DIC***	***3D-DIC***	***2D-DIC***	***3D-DIC***	***2D-DIC***	***3D-DIC***	***2D-DIC***
DP800-UT-1	*0.559*	*0.554*	*-0.187*	*-0.194*	*0.569*	*0.562*	*0.434*	*0.427*
DP800-UT-2	*0.518*	*0.530*	*-0.176*	*-0.180*	*0.527*	*0.539*	*0.431*	*0.430*
DP800-UT-3	*0.527*	*0.531*	*-0.189*	*-0.192*	*0.534*	*0.537*	*0.421*	*0.417*
Avg.	***0.535***	***0.538***	***-0.184***	***-0.188***	***0.543***	***0.546***	***0.428***	***0.425***
Std. Dev.	***0.021***	***0.014***	***0.007***	***0.008***	***0.022***	***0.014***	***0.007***	***0.007***

Table A3: Fracture strains obtained from 2D-DIC and stereo DIC (3D) for PST tests for CR4 steel								
Property	***Major Strain*** ε_{Major}		***Minor Strain*** ε_{Minor}		***Effective Strain*** $\varepsilon_{Effective\ von\ Mises}$		***Stress Triaxiality***	
Sample	***3D-DIC***	***2D-DIC***	***3D-DIC***	***2D-DIC***	***3D-DIC***	***2D-DIC***	***3D-DIC***	***2D-DIC***
CR4-PST-1	*0.730*	*0.724*	*-0.157*	*-0.160*	*0.768*	*0.761*	*0.493*	*0.491*
CR4-PST-2	*0.723*	*0.729*	*-0.150*	*-0.152*	*0.763*	*0.769*	*0.495*	*0.495*
CR4-PST-3	*0.733*	*0.726*	*-0.159*	*-0.159*	*0.772*	*0.763*	*0.493*	*0.492*
Avg.	***0.728***	***0.726***	***-0.155***	***-0.157***	***0.768***	***0.764***	***0.494***	***0.493***
Std. Dev.	***0.005***	***0.002***	***0.005***	***0.004***	***0.004***	***0.004***	***0.001***	***0.002***

Table A4: Fracture strains obtained from 2D-DIC and stereo DIC (3D) for UT tests for DP800 steel								
Property	***Major Strain*** ε_{Major}		***Minor Strain*** ε_{Minor}		***Effective Strain*** $\varepsilon_{Effective\ von\ Mises}$		***Stress Triaxiality***	
Sample	***3D-DIC***	***2D-DIC***	***3D-DIC***	***2D-DIC***	***3D-DIC***	***2D-DIC***	***3D-DIC***	***2D-DIC***
DP800-PST-1	*0.405*	*0.404*	*-0.028*	*-0.028*	*0.453*	*0.451*	*0.554*	*0.554*
DP800-PST-2	*0.390*	*0.373*	*-0.028*	*-0.028*	*0.435*	*0.415*	*0.554*	*0.553*
DP800-PST-3	*0.392*	*0.388*	*-0.029*	*-0.027*	*0.436*	*0.433*	*0.554*	*0.554*
Avg.	***0.396***	***0.388***	***-0.029***	***-0.028***	***0.441***	***0.433***	***0.554***	***0.553***
Std. Dev.	***0.008***	***0.015***	***0.001***	***0.001***	***0.010***	***0.018***	***0.000***	***0.001***

Table A5: Fracture strains obtained from 2D-DIC and stereo DIC (3D) for SH tests for CR4 steel								
Property	***Major Strain*** ε_{Major}		***Minor Strain*** ε_{Minor}		***Effective Strain*** $\varepsilon_{Effective\ von\ Mises}$		***Stress Triaxiality***	
Sample	***3D-DIC***	***2D-DIC***	***3D-DIC***	***2D-DIC***	***3D-DIC***	***2D-DIC***	***3D-DIC***	***2D-DIC***
CR4-SH-1	*1.064*	*1.037*	*-0.868*	*-0.827*	*1.132*	*1.097*	*0.111*	*0.119*
CR4-SH-2	*1.017*	*1.047*	*-0.795*	*-0.839*	*1.070*	*1.109*	*0.135*	*0.126*
CR4-SH-3	*1.047*	*1.059*	*-0.843*	*-0.858*	*1.110*	*1.125*	*0.129*	*0.124*
Avg.	***1.043***	***1.048***	***-0.835***	***-0.841***	***1.104***	***1.110***	***0.125***	***0.123***
Std. Dev.	***0.024***	***0.011***	***0.037***	***0.016***	***0.032***	***0.014***	***0.012***	***0.004***

Table A6: Fracture strains obtained from 2D-DIC and stereo DIC (3D) for SH tests for DP800 steel								
Property	***Major Strain*** ε_{Major}		***Minor Strain*** ε_{Minor}		***Effective Strain*** $\varepsilon_{Effective\ von\ Mises}$		***Stress Triaxiality***	
Sample	***3D-DIC***	***2D-DIC***	***3D-DIC***	***2D-DIC***	***3D-DIC***	***2D-DIC***	***3D-DIC***	***2D-DIC***
DP800-SH-1	*0.624*	*0.590*	*-0.549*	*-0.513*	*0.681*	*0.641*	*0.075*	*0.074*
DP800-SH-2	*0.603*	*0.606*	*-0.528*	*-0.535*	*0.657*	*0.662*	*0.078*	*0.072*
DP800-SH-3	*0.583*	*0.576*	*-0.521*	*-0.514*	*0.640*	*0.632*	*0.056*	*0.063*
Avg.	***0.603***	***0.590***	***-0.533***	***-0.521***	***0.659***	***0.645***	***0.070***	***0.069***
Std. Dev.	***0.020***	***0.015***	***0.014***	***0.013***	***0.021***	***0.016***	***0.012***	***0.006***

Table A7: Fracture strains from 2D-DIC, stereo DIC (3D) and out-of-plane compensated 2D-DIC for BBT tests for CR4 steel

Property	***Major Strain*** ε_{Major}			***Minor Strain*** ε_{Minor}			***Effective Strain*** $\varepsilon_{Effective\ von\ Mises}$			***Stress Triaxiality***	
Sample	**3D**	**2D**	**2D(C)**	**3D**	**2D**	**2D(C)**	**3D**	**2D**	**2D(C)**	**3D**	**2D**
CR4-BBT-1	*0.338*	*0.394*	*0.352*	*0.347*	*0.402*	*0.361*	*0.685*	*0.796*	*0.713*	*0.667*	*0.667*
CR4-BBT-2	*0.368*	*0.424*	*0.381*	*0.383*	*0.441*	*0.399*	*0.751*	*0.865*	*0.781*	*0.667*	*0.667*
CR4-BBT-3	*0.422*	*0.461*	*0.420*	*0.415*	*0.457*	*0.416*	*0.837*	*0.919*	*0.835*	*0.667*	*0.667*
Avg.	***0.376***	***0.426***	***0.384***	***0.382***	***0.433***	***0.392***	***0.758***	***0.860***	***0.776***	***0.667***	***0.667***
Std. Dev.	***0.043***	***0.034***	***0.034***	***0.034***	***0.028***	***0.028***	***0.077***	***0.061***	***0.061***	***0.000***	***0.000***

Table A8: Fracture strains from 2D-DIC, stereo DIC (3D) and out-of-plane compensated 2D-DIC for BBT tests for DP800 steel

Property	***Major Strain*** ε_{Major}			***Minor Strain*** ε_{Minor}			***Effective Strain*** $\varepsilon_{Effective\ von\ Mises}$			***Stress Triaxiality***	
Sample	**3D**	**2D**	**2D(C)**	**3D**	**2D**	**2D(C)**	**3D**	**2D**	**2D(C)**	**3D**	**2D**
DP800-BBT-1	*0.231*	*0.273*	*0.232*	*0.210*	*0.254*	*0.213*	*0.441*	*0.528*	*0.446*	*0.666*	*0.667*
DP800-BBT-2	*0.200*	*0.243*	*0.202*	*0.211*	*0.254*	*0.213*	*0.411*	*0.497*	*0.415*	*0.667*	*0.667*
DP800-BBT-3	*0.231*	*0.277*	*0.235*	*0.233*	*0.279*	*0.237*	*0.464*	*0.556*	*0.472*	*0.667*	*0.667*
Avg.	***0.221***	***0.264***	***0.223***	***0.218***	***0.262***	***0.221***	***0.439***	***0.527***	***0.444***	***0.667***	***0.667***
Std. Dev.	***0.018***	***0.018***	***0.018***	***0.013***	***0.014***	***0.014***	***0.027***	***0.029***	***0.028***	***0.000***	***0.000***

REFERENCES

1. Agha, A. and F. Abu-Farha, *Numerical implementation and validation of a viscoelastic-plastic material model for predicting curing induced residual stresses in adhesive bonded joints.* International Journal of Adhesion and Adhesives, 2022. **118**: p. 103195.
2. Esmaeilpour, R., et al., *Effect of hardening law and process parameters on finite element simulation of single point incremental forming (SPIF) of 7075 aluminum alloy sheet.* Mechanics & Industry, 2020. **21**(3): p. 302.
3. Nazzal, M., et al., *Wrinkling suppression in thin membranes using designed geometrical features.* Proceedings of the Institution of Mechanical Engineers, Part C: Journal of Mechanical Engineering Science, 2022. **236**(19): p. 10163-10174.
4. Agha, A. and F. Abu-Farha, *Experimental methods to capture curing induced effects in adhesive bonded joints.* International Journal of Adhesion and Adhesives, 2021. **104**: p. 102735.
5. Agha, A. and F. Abu-Farha, *Advanced Anti-Buckling Device Coupled with Real-Time Digital Image Correlation for Complex Cyclic Tension-Compression Testing of Lightweight Materials.* 2022: p. 40-54.
6. Andrade, F.X.C., Feucht, M., Haufe, A., Neukamm, F., *An incremental stress state dependent damage model for ductile failure prediction.* International Journal of Fracture, 2016. **200**(1-2): p. 127-150.
7. Wierzbicki, T., et al., *Calibration and evaluation of seven fracture models.* International Journal of Mechanical Sciences, 2005. **47**(4-5): p. 719-743.
8. Bai, Y. and T. Wierzbicki, *Application of extended Mohr–Coulomb criterion to ductile fracture.* International Journal of Fracture, 2009. **161**(1): p. 1-20.
9. Jia, Y. and Y. Bai, *Ductile fracture prediction for metal sheets using all-strain-based anisotropic eMMC model.* International Journal of Mechanical Sciences, 2016. **115-116**: p. 516-531.
10. Jun Hu, G.T., Cynthia Campbell, *True Fracture Strain Measurement and Derivation for GISSMO Calibration.* WCX SAE World Congress Experience, 2022.
11. Li, J., et al., *A method of the direct measurement of the true stress–strain curve over a large strain range using multi-camera digital image correlation.* Optics and Lasers in Engineering, 2018. **107**: p. 194-201.
12. Murienne, B.J. and T.D. Nguyen, *A comparison of 2D and 3D digital image correlation for a membrane under inflation.* Opt Lasers Eng, 2016. **77**: p. 92-99.
13. Mohr, D. and F. Ebnoether, *Plasticity and fracture of martensitic boron steel under plane stress conditions.* International Journal of Solids and Structures, 2009. **46**(20): p. 3535-3547.
14. Roth, C.C. and D. Mohr, *Effect of strain rate on ductile fracture initiation in advanced high strength steel sheets: Experiments and modeling.* International Journal of Plasticity, 2014. **56**: p. 19-44.
15. Lianxiang Yang, L.S., Abhishek Gothekar, Xu Chen, *Measure Strain Distribution Using Digital Image Correlation (DIC) for Tensile Tests.* The Advanced High Strength Steel Stamping Team of the Auto/Steel Partnership (A/SP), January 30, 2010.
16. Charoensuk, K., S. Panich, and V. Uthaisangsuk, *Damage initiation and fracture loci for advanced high strength steel sheets taking into account anisotropic behaviour.* Journal of Materials Processing Technology, 2017. **248**: p. 218-235.
17. Sutton, M.A., et al., *The effect of out-of-plane motion on 2D and 3D digital image correlation measurements.* Optics and Lasers in Engineering, 2008. **46**(10): p. 746-757.
18. Pan, B., L. Yu, and D. Wu, *High-Accuracy 2D Digital Image Correlation Measurements with Bilateral Telecentric Lenses: Error Analysis and Experimental Verification.* Experimental Mechanics, 2013. **53**(9): p. 1719-1733.
19. Pan, B., L. Yu, and D. Wu, *High-accuracy 2D digital image correlation measurements using low-cost imaging lenses: implementation of a generalized compensation method.* Measurement Science and Technology, 2014. **25**(2): p. 025001.

20. Bai, P., F. Zhu, and X. He, *Optical extensometer and elimination of the effect of out-of-plane motions.* Optics and Lasers in Engineering, 2015. **65**: p. 28-37.
21. Hoult, N.A., et al., *Experimental accuracy of two dimensional strain measurements using Digital Image Correlation.* Engineering Structures, 2013. **46**: p. 718-726.
22. Wittevrongel, L., et al., *Evaluation of Methodologies for Compensation of Out of Plane Motions in a 2D Digital Image Correlation Setup.* Strain, 2015. **51**(5): p. 357-369.
23. Xu, X., et al., *High-Accuracy, High-Efficiency Compensation Method in Two-Dimensional Digital Image Correlation.* Experimental Mechanics, 2017. **57**(6): p. 831-846.
24. Zhao, J., Y. Sang, and F. Duan, *The state of the art of two-dimensional digital image correlation computational method.* Engineering Reports, 2019. **1**(2).
25. Hu, J., *Characterization and modeling of deformation, springback, and failure in advanced high strength steels (AHSSs).* All Dissertations, 2016. **1840**.